JOINT EUROPEAN TORUS

JET–P(92)75

M. Sasao, J.M. Adams, S. Conroy, O.N. Jarvis, F.B. Marcus, G. Sadler,
P. van Belle and JET Team

Determination of the Ion Thermal Diffusivity from Neutron Emission Profiles in Decay

Determination of the Ion Thermal Diffusivity from Neutron Emission Profiles in Decay

M. Sasao[1], J.M. Adams[2], S. Conroy, O.N. Jarvis, F.B. Marcus, G. Sadler, P. van Belle and JET Team*

JET-Joint Undertaking, Culham Science Centre, OX14 3DB, Abingdon, UK

[1]National Institute for Fusion Science, Nagoya-464, Japan
[2]AEA Industrial Technology, Harwell Laboratory, Oxon, OXll ORA
** See Annex*

Preprint of Paper to be submitted for publication in
Plasma Physics and Controlled Fusion

ABSTRACT.

Spatial profiles of the neutron emission from deuterium plasmas are routinely obtained at the Joint European Torus (JET) using the line-integrated signals measured with a multi-channel instrument. It is shown that the manner in which these profiles relax following the termination of strong heating with Neutral Beam Injection (NBI) permits the local thermal diffusivity (χ_i) to be obtained with an accuracy of about 20%. The profiles of χ_i for small minor radius ($r/a < 0.6$) were found to be fiat and to take values between 0.3 and 1.1 m^2s^{-1} for H-mode plasmas with plasma current I_p = 3.1MA and toroidal field B_T = 2.3T. The value of χ_i was smallest for Z_{eff} = 2.2 and increased weakly with increasing Z_{eff}. The predictions of neoclassical theory are much smaller than the experimental values for low Z_{eff} but increase rapidly until they become comparable with the experimental values at the highest Z_{eff} obtained.

1. Introduction

Recent progress in profile measurements of plasma properties has permitted studies of plasma transport to be carried out in increasing detail. Various types of discharge have been intensively analyzed, especially at JET [1-4], in studies of local transport properties. Work at JET, TFTR, and JT-60 etc. [1-6] on the local energy balance during the neutral beam heating phase, using interpretative codes, has relied on charge-exchange recombination spectroscopy to provide the ion temperature profiles. The main loss terms in the ion power balance for the central region in these cases were the ion heat conduction and the ion-electron equipartition. The main source term was the input power from auxiliary heating. The value of the ion thermal conductivity thus obtained depends very much on the estimation of the beam deposition, which was calculated using density, temperature and impurity profile data. The estimated uncertainties associated with the deduced thermal diffusivities were usually about 50% [1].

Esposito et al. [7] have also obtained the local ion thermal conductivity of JET plasmas during ohmic and ion cyclotron resonance heating phases. They used the JET neutron profile monitor [8] to determine the ion temperature profile. Here the equipartition term, due to the temperature difference between ions and electrons, was the main contributor to the ion heating. The values of the ion thermal conductivity so obtained had uncertainties of more than a factor of two.

We have studied the "after-glow" behaviour of beam-heated JET plasmas, i.e. the behaviour of the neutron emission just after the beam heating has been switched off. In this phase, the ion stored energy is decreasing gradually, mainly due to the effects of the ion thermal conductivity. The neutron emission profile data were analyzed to obtain the decay rate of the ion stored energy. There was no additional heating power and the equipartition and the other terms contributed very little. In the following section, the power balance for this phase will be presented and the analysis procedure will be outlined. In section 3, χ_i profiles of some discharges from the autumn campaign of 1990 are presented. Values are obtained for the ion diffusivity χ_i with a rather small uncertainty (about ± 20%). Finally, in section 4, the Z_{eff} dependence is compared with the prediction of neoclassical theory.

2. Data analysis procedure

The JET neutron profile monitor views the plasma along 19 chords (10 horizontal and 9 vertical), giving line-of-sight integrated neutron emissivities [8]. Fig. 1 shows an example of the time evolution of the neutron emission measured by the central chord (channel 5) and by the uppermost chord (channel 1) of the horizontal camera during and after the neutral beam injection period. At the termination of NBI, the neutron emission started to decay. As there was no significant MHD activity, the neutron decay rate immediately following NBI termination was essentially given by that of the beam-plasma interactions, assuming classical slowing down of the beam particles. After the beam particles had thermalized, only the cooling of the thermal plasma ions contributed to the decay of the neutron emission. This is the time domain of present interest.

The local ion power balance can be generally expressed as

$$\frac{dW_i}{dt} = Q_{ei} - Q_{conv} - Q_{cx} - Q_{cond} + Q_H \qquad (1)$$

The last term represents the additional heating power input, which is zero in the present case. The 2nd, and 3rd terms, representing the losses due to convection and charge exchange, were considered to be negligible since a full analysis of the JET beam heated plasmas [2] shows that these terms are much smaller than the conduction term in the central region. Following cessation of NBI, the neutral particle density, the origin of the convection and charge exchange loss terms, will be considerably reduced. The local power balance for the scenario considered here is as follows, for the geometrical approximation of a one-dimensional, cylindrical plasma:

$$\frac{dW_i}{dt} = Q_{ei} - Q_{cond}$$

$$= \frac{3}{2}\frac{n_e (T_e - T_i)}{\tau_{ei}} + \frac{1}{r}\frac{\partial}{\partial r}\{r\, n_i(r)\, \chi_i(r) \frac{\partial T_i}{\partial r}\} \qquad (2)$$

In the present work, the ion temperature profile $T_i(r)$ and the change of the ion stored energy W_i were provided by the neutron profile monitor. The line-integrated neutron emissions recorded along the 19 chords were analyzed by means of the ORION code [9]. This assumes that the magnetic flux surfaces are

contours of constant neutron emissivity, $Y_n(\rho)$, which is described in terms of a given functional form. The normalized radius on the midplane, ρ, is used as the flux surface label. Esposito et al. [7] have extensively studied the quality of the fit to the data given by various functions and concluded that the derived ion temperature profile was not particularly affected by the choice of the fitting function.

We have used a parabolic function:

$$Y_n(r) = Y_n(0)\,(1-\rho^2)^{\alpha}$$

The parameter α was determined by the fitting procedure to an accuracy of between 5 and 20 %. The relationship between neutron emission rate and ion temperature can be expressed as

$$Y_n = \frac{1}{2}\{ n_d^2\, T_i^{\beta} \} \tag{3}$$

Treating β as being a constant, the rate of change in the local neutron emissivity can be related to changes in the ion temperature and deuteron density as

$$\frac{dY_n}{dt} = \frac{1}{2}\{ \beta\, n_d^2\, T_i^{\beta-1}\, \frac{\partial T_i}{\partial t} + 2\, n_d\, T_i^{\beta}\, \frac{\partial n_d}{\partial t} \} \tag{4}$$

The parameter β varies weakly, from 3.5 to 2.9 for a temperature variation from 3 to 8 keV. The rate of change in the ion stored energy is

$$\frac{dW_i}{dt} = \frac{3}{2}\{ n_d \frac{\partial T_i}{\partial t} + T_i \frac{\partial n_d}{\partial t} \} \tag{5}$$

Combining (2), (4) and (5), the rate of change in the ion stored energy can be expressed by

$$\frac{1}{W_i}\frac{dWi}{dt} = \frac{1}{\beta}\frac{1}{Y_n}\frac{\partial Y_n}{\partial t} + (1-2/\beta)\,\frac{1}{n_d}\,\frac{\partial n_d}{\partial t} \tag{6a}$$

$$= \frac{n_e\,(T_e-T_i)}{\tau_{ei}\, n_d\, T_i} + \frac{2}{3\, n_d\, T_i}\frac{1}{r}\,\frac{\partial}{\partial r}[r\, n_d(r)\, \chi_i(r)\, \frac{\partial T_i(r)}{\partial r}] \tag{6b}$$

These two equations are used to obtain χ_i in this work.

During the time interval of the analysis, the changes in the plasma properties were moderate except for the change of the neutron emission, which is shown in fig. 1. Because the change in n_e and Z_{eff} is normally small, the second term of the right side in eq. (6a) is almost an order of magnitude smaller than the first. As will be shown later, the contribution from the first term of eq. (6b) is also small. For the remaining terms of eqs. (6a) and (6b), only relative rates of changes in n_d, T_i, and Y_n are needed. The neutron emission decay constant,

$$\frac{1}{Y_n}\frac{dY_n(\rho)}{dt}$$

and the profile peaking factor for T_i are the main quantities needed for the determination of χ_i.

The decay rate of the local neutron emissivity, $\delta Y_n(r)/\delta t$, was obtained with the ORION code at 100 ms time intervals; a typical radial profile, $Y_n(r)$, is shown in fig.2. The profile of the decay constant for discharge 22871 is shown in fig. 3. The decay constants of the neutron brightness along each of the 19 chords are also shown; the profile of the decay constant is rather flat, which could have been anticipated from the fact that the profile parameter α did not change appreciably during the decay phase, as is seen in fig. 2.

An example of the ion temperature profile obtained from the neutron profile monitor is shown in fig. 4, together with T_e (ECE) and n_e (interferometer) profiles. The validity of the latter two quantities was confirmed by LIDAR measurements [10]. The deuteron density $n_d(r)$ was calculated from the comparison of $T_i(0)$ measured with the crystal spectrometer and the central neutron emissivity, assuming a uniform dilution factor n_d/n_e. When the quality of the $T_i(0)$ data provided by the crystal spectrometer was poor, $n_d(r)$ was obtained from $n_e(r)$ (interferometer, or LIDAR) and Z_{eff} with the impurity distribution of Be : C : O : Ni = 4 :1 : 0.5 : 0.2.

The three terms of the power balance equation, eq.(2), are shown in fig. 5 for the same discharge. The contribution of the equipartition term was usually small because the electron and ion temperatures did not differ greatly at this stage.

3. Experimental Results

In order to study the ion transport by analyzing the decaying neutron emission profile, the following restrictions must be observed,

i) A statistically significant number of counts ($> 10^2$) is required for each channel of the neutron profile monitor in order to obtain useable ion temperature profiles and local neutron decay constants.

ii) A sharp termination of more than 5 MW of additional heating is preferable. A short slowing down time of the beam particles (low injection energy, for example) is also desirable.

iii) There should not be any significant MHD activity, such as sawteeth, which might expel high energy particles from the central region of the plasma.

These criteria led to the selection of just 13 discharges from the 1990 autumn campaign. Discharge 20222 of the 1989 campaign was included as a reference case. The χ_i profile was obtained by solving eqs. (6a, 6b). The results, $\chi_i(0.3a)$ and $\chi_i(0.5a)$, are listed in table 1, along with the discharge type, time into the discharge, I_P, B_T, $n_e(0)$, $T_i(0)$, and Z_{eff}. Discharges 22336 to 22370 were high-performance double-null discharges, and discharges 22866 to 22890 were single-null (upper) discharges for H-mode studies.

When considering the experimental errors, the following items were taken into account:

1) the peaking factor in the neutron profile,
2) the decay constant of neutron emission,
3) the peaking factor in the electron density,
4) the local electron and the ion temperature.

The 4th item contributes little, in spite of the 30% uncertainties associated with the electron and ion temperatures. This is because the equipartition term is usually small compared with other two terms, as can be seen in fig. 5.

The upper and lower levels of the χ_i profiles in Fig. 6 indicate the regions of $\chi_i \pm \Delta\chi_i$ for 22871 and 22874. The abscissa shows the radial co-ordinate, r/a, quoted as the middle value for the finite region viewed (± 5 cm). These results were obtained assuming a parabolic form for the neutron emission profiles; this form is most reliable for the r/a range from 0.25 to 0.55, where the gradient is strong and easily parametized. The measured profiles are not sensitive to the actual gradients over the central region, for which the assumption of a parabolic form is probably incorrect.

The interfering signal due to 14 MeV neutrons arising from the burn-up of the 1.0 MeV tritons emitted in the alternative branch of the d-d fusion reaction [11]

was considered to be sufficiently small that they could be neglected under the circumstances of the measurements reported here, where the neutron emission has fallen by only one order of magnitude from the peak rates. The total 14 MeV neutron emission strength is about 1% of the 2.5 MeV strength under steady-state conditions; the detection efficiency for 14 MeV neutrons is about 25% of that for 2.5 MeV neutrons. The absence of serious contamination was confirmed by the fact that pulse height distributions recorded by the neutron detectors during the decay phase were very similar to those recorded during NBI heating.

4. Discussion

Although the χ_i profiles obtained in this work are limited to the region of $0.25 < r/a < 0.55$ and apply only during the decaying phase in the absence of additional heating, some interesting features are seen. First of all, the derived χ_i values range from 0.3 to 1 m^2/s and are comparable with results obtained by other workers [1-7]. Secondly, the χ_i profiles are almost flat. This is seen in fig.6 for two selected discharges but is also true for all the cases presently analyzed, as indicated in table 1. The flat χ_i profile has also been obtained in the beam heated plasma of a medium density H-mode discharge with similar parameters, while a low density hot ion mode discharge showed an increase in the outer region [1].

A comparison between the predictions of the neoclassical theory, χ_i^{neo}, and the present results, χ_i^{exp}, has been made. The formula given by Chang and Hinton [12], which includes finite aspect ratio effects and enhanced collisionality due to impurity ions, has been used. Only one impurity component, carbon, was considered. In fig. 6, the dashed line, indicating χ_i^{neo}, is much smaller than χ_i^{exp} for discharge 22871, but in the case of discharge 22874 (which is very similar to discharge 22871 except for the larger Z_{eff}), the χ_i^{exp} values approach χ_i^{neo}. However, the experimental and calculated profile shapes differ for both cases. The theoretical models of ion temperature gradient driven turbulence (η_i-mode) were tested in the parameter range $0.5 < \eta_i < 4.5$. The experimental χ_i values are typically two orders of magnitude smaller than the theoretical predictions [13]. The flat χ_i profiles of the present analysis also disagree with the theoretical predictions in that they do not show any major changes near η_{crit}. Disagreement with the η_i mode have also been reported for various auxiliary heated plamas in JET [3-4].

In order to show the Z_{eff} dependence, the χ_i^{exp} (r/a=0.3) values are plotted against Z_{eff} in fig.7, for discharges between 22866 and 22890. All of these discharges were single-null discharges with I_P=3.1 MA. The plasmas of these

discharges during the decay phase under investigation were apparently still in the H-mode before undergoing the transition back to L-mode. Gas introduction had been terminated earlier. The χ_i^{exp} (r/a=0.3) values appear to rise gradually with increasing Z_{eff}. The same tendency was seen at r/a=0.5. The dashed line in Fig. 7, connecting the calculated χ_i^{neo} values, lies appreciably below the experimental points for low Z_{eff} but rises above the experimental points for high Z_{eff}. No "anomalous" effects due to turbulence were identified.

Two points obtained with higher toroidal fields are also plotted in fig.7. The predictions of neoclassical theory give lower values than the B_T=2.3 T line, while the experimental points are a little higher. However, the uncertainties from the present analysis are too large for any useful conclusion to be drawn regarding the difference.

5. Conclusion

The present work has shown that analysis of the neutron emission profiles taken during the decay period following abrupt termination of NBI heating can be exploited for measurements of the thermal ion conductivity. The χ_i profiles that were obtained were rather flat over the region of $0.25 < r/a < 0.55$, as was found for the beam heated plasma of a medium density H-mode discharge, in spite of the difference in the main terms of the ion power balance. A weak dependence on Z_{eff} can be seen in the data, with the experimental values for χ_i coinciding with the neoclassical predictions only at high Z_{eff}.

Acknowledgements

The authors greatly appreciate discussions held with B.Balet, D.J.Campbell and M.von Hellermann. They wish to acknowledge the contributions of other members of the JET team, who made the experiments possible as well as providing experimental data and results of calculation. A discussion with K.Itoh was also greatly appreciated. One of the authors (M.Sasao) would like to acknowledge the financial support from Japanese Society of Science Promotion.

References

[1] WATKINS, M.L, et al., Plasma Physics and Controlled Fusion 31 (1990) 1713.

[2] BALET,B., BOYD,D.A., CAMPBELL,D.J., et al., Nucl. Fusion 30 (1990) 2029.

[3] BALET,B., et al., Proc. of 17th EPS Conference on Controlled Fusion and Plasma heating, Amsterdam, 1990. Vol.1, p162.

[4] TIBONE,F., et al., Proc. of 17th EPS Conference on Controlled Fusion and Plasma heating, Amsterdam, 1990. Vol.2, p805.

[5] ZARNSTORFF,M., et al., 12th Int. Conf. on Plasma Physics and Controlled Nuclear Fusion Research, IAEA-CN-50/A-3-3 (Nice,1988).

[6] HIRAYAMA,T., et al., Nuclear Fusion Research (KAKUYUGO-KENKYU), Vol.65 Supp. (1991), 75

[7] ESPOSITO,B., MARCUS, F.B., ADAMS,J.M., et al., Proceedings of 18th European Conference on Controlled Fusion and Plasma Physics (Berlin,1991), IV-277.

[8] ADAMS,J.M., CHEETHAM.A., CONROY,S., et al., in Controlled Fusion and Plasma Physics (Proc. 16th Eur. Conf. Venice, 1989) Vol.13B, Part I, European Physical Society (1989) 63.

[9] CONROY,S., Diagnosis of Fusion Products for Reactor Relevant Plasmas, Ph. D. Thesis, Imperial College, London (1990)

[10] SALZMANN,H., HIRSCH,K., NIELSEN,P., et al, Nuclear Fusion 27 (1987) 1925.

[11] JARVIS,O.N., ADAMS,J.M., CONROY,S., MARCUS,F.B., SADLER,G.J., WATKINS,N., VAN BELLE, P. Proceedings of 18th European Conference on Controlled Fusion and Plasma Physics (Berlin,1991), I-21.

[12] CHANG,C.S., HINTON,F.L., Phys. Fluids 29 (1986) 3314.

[13] DOMINGUEZ,R.R. and WALTZ,R.E., Nuclear Fusion 27 (1987) 65.

Table 1

Plasma parameters and $\chi_i(0.3a)$, $\chi_i(0.5a)$ for the discharges analyzed. DX and UX indicate discharges of double-null and upper-null configurations, respectively. $T_i(0)$ was obtained either from Ni line broadening using the crystal spectrometer or from the neutron emission rate. Z_{eff} was calculated from the comparison of $T_i(0)$ measured with the crystal spectrometer and the neutron emissivity, assuming the impurity distribution of Be : C : O : Ni = 4 : 1 : 0.5 : 0.2. When the $T_i(0)$ data were of doubtful quality, the Bremsstrahlung Z_{eff} results were tabulated.

Shot	Type	Time	I_P(MA)	B_T(T)	$n_e(0)$	$T_i(0)$	Z_{eff}	$\chi_i(0.3)$	$\chi_i(0.5)$
20222	UX	11.2	4.0	2.90	0.4	3.5	2.2	0.86±0.17	1.04±0.26
22336	DX	15.8	3.6	2.90	0.4	6.0	2.2	0.34±0.08	0.43±0.12
22343	DX	13.55	3.7	3.45	0.3	4.5	2.6	0.42±0.12	0.47±0.12
22344	DX	14.2	3.7	3.45	0.2	4.6	3.5	0.89±0.16	1.02±0.20
22370	DX	16.25	3.0	2.27	0.3	5.2	4.5	1.00±0.40	0.95±0.30
22866	UX	12.7	3.1	2.27	0.4	4.1	6.1	0.97±0.20	1.04±0.24
22871	UX	12.7	3.1	2.27	0.4	6.5	2.2	0.37±0.05	0.45±0.13
22874	UX	12.55	3.1	2.27	0.5	3.8	4.3	0.56±0.17	0.58±0.22
22877	UX	13.2	3.1	2.89	0.4	5.1	5.3	0.75±0.15	0.81±0.15
22878	UX	13.2	3.1	3.45	0.3	5.4	2.8	0.54±0.08	0.61±0.12
22883	UX	14.7	3.1	2.28	0.3	5.1	3.5	0.44±0.12	0.54±0.15
22884	UX	14.7	3.1	2.28	0.4	4.9	2.2	0.36±0.05	0.44±0.10
22888	UX	13.2	3.1	2.27	0.5	3.9	5.3	0.58±0.18	0.58±0.29
22890	UX	15.2	3.1	2.27	0.6	4.5	2.6	0.34±0.07	0.37±0.12

Time is given in seconds, $n_e(0)$ in units of 10^{20} m^{-3} and $T_i(0)$ in keV.

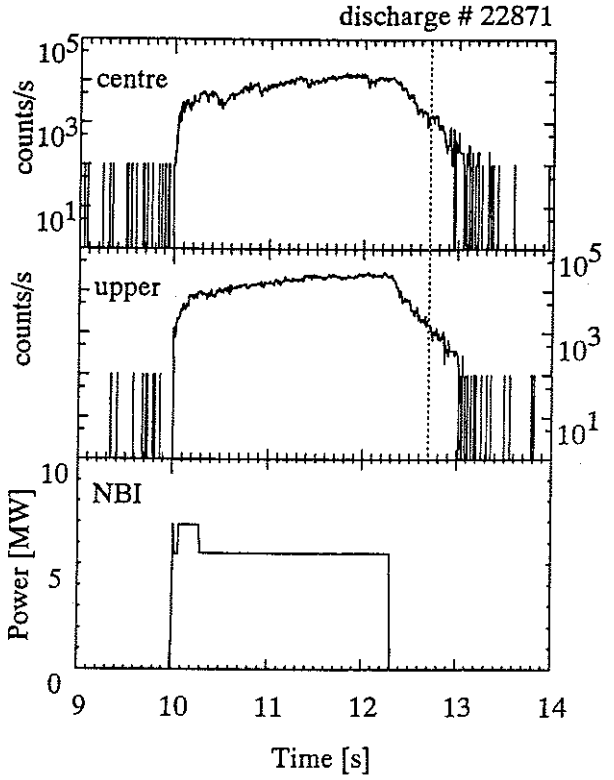

Fig. 1: Showing the time evolution of the neutron emissivity recorded by the central and upper-most chords, together with the input power of the 80 keV neutral beam for discharge 22871.

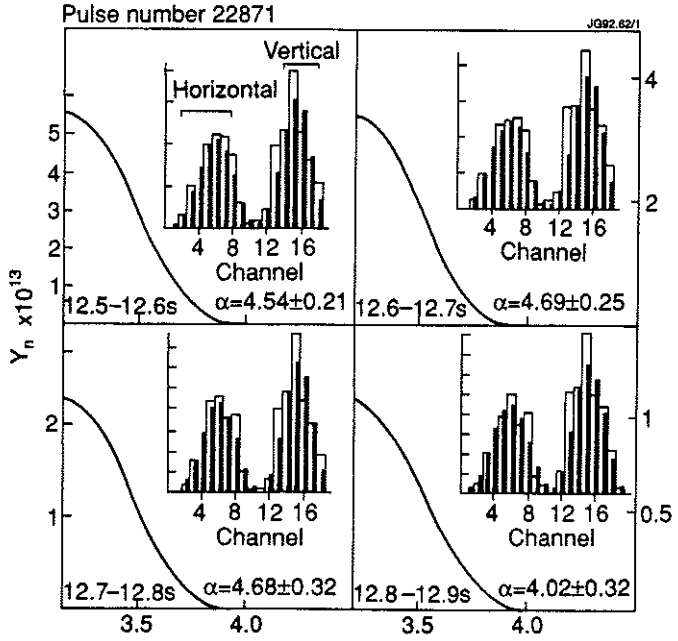

Fig. 2. The fitted neutron emissivity profile for each 100 ms (from 12.5 to 12.9 s) in the decay phase of discharge 22871. The measured neutron brightness versus channel number are also compared with the fitted brightness (solid bars). Channels 1 to 10 represent measurements along approximately horizontal chords, channels 11 to 19 to approximately vertical chords. Channel 4 in the horizontal camera was excluded from the fitting.

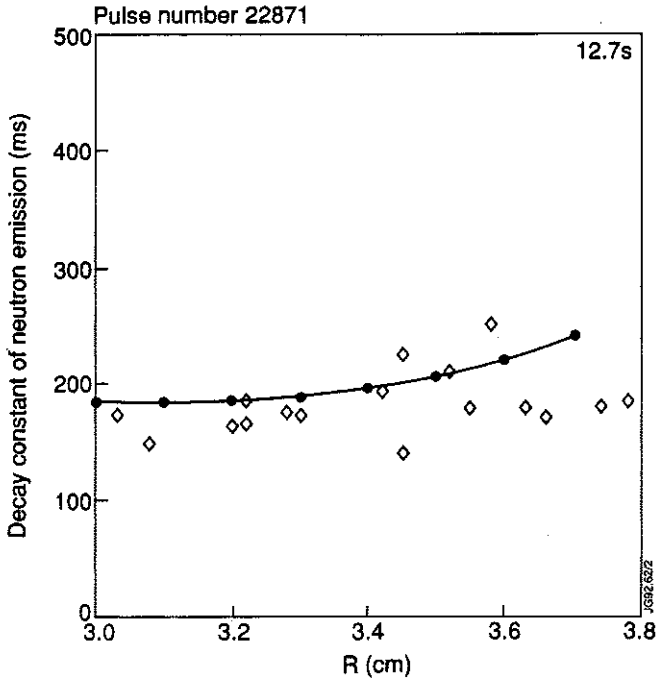

Fig. 3. The profile of the decay constant in the decay phase of discharge 22871. The decay constants of the neutron brightness for each of the 19 chords are also shown with diamonds. Each data point is plotted at the position corresponding to the highest neutron emissivity along the line of sight for that channel. Points connected with a solid line are those obtained after fitting with the ORION code.

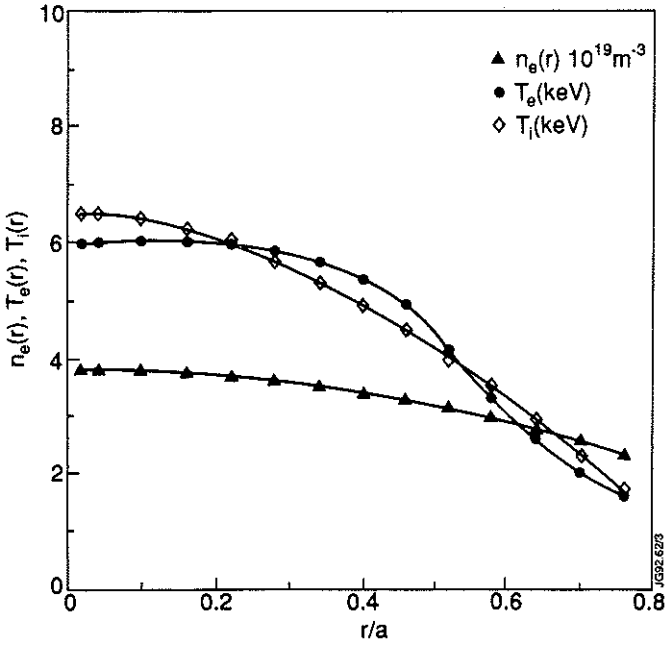

Fig. 4. T_i (neutron profile monitor), T_e (ECE) and n_e(interferometer) profiles at 12.7 sec into discharge 22871.

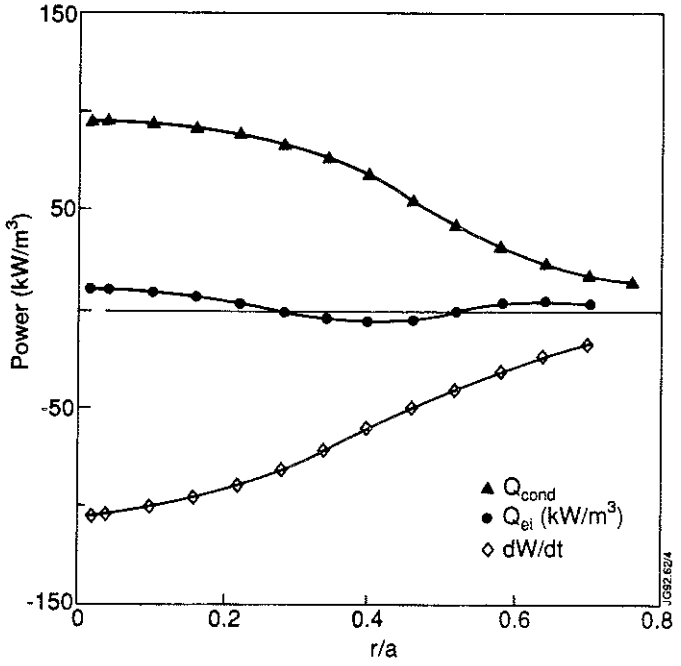

Fig. 5. The power balance for the decay phase of the discharge 22871. The contribution from the equipartition term is much smaller than other two and the conduction term can be estimated mainly from the change in the ion stored energy, which is determined from the decay rate of the neutron emissivity.

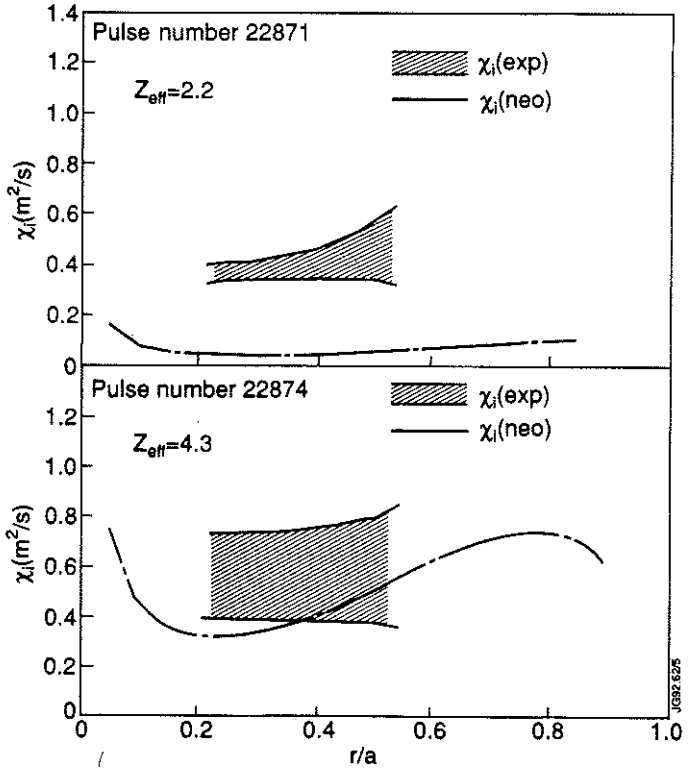

Fig.6. The χ_i profiles for discharges 22871(upper) and 22874(lower). The hatched areas indicate the regions of $\chi_i+\Delta\chi_i$. The neoclassical χ_i profiles are indicated by dashed lines.

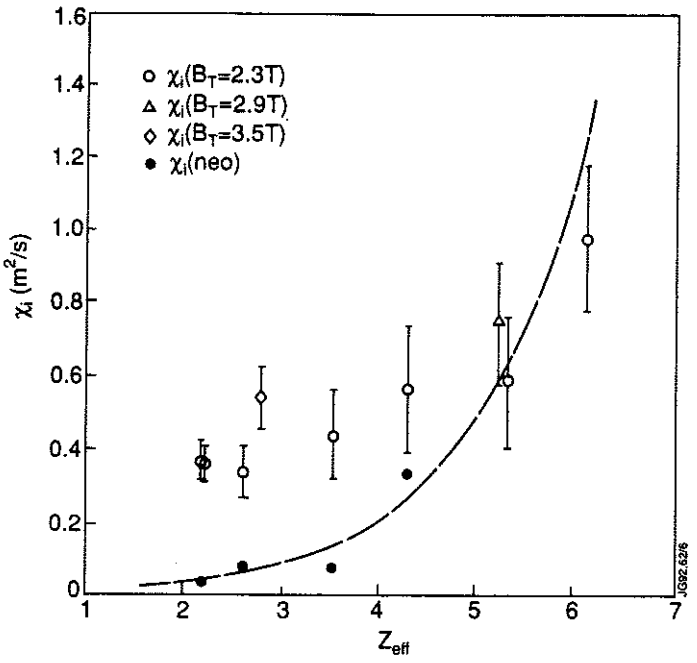

Fig.7. The Z_{eff} dependence of $\chi_i^{exp}(r/a=0.3)$ values for discharges 22866 to 22890, which were single null discharges with Ip=3.1A. The values of Z_{eff} have associated uncertainties of about 30%. The dashed line connects the calculated χ_i^{neo} values.

Appendix I

THE JET TEAM

JET Joint Undertaking, Abingdon, Oxon, OX14 3EA, U.K.

J.M. Adams[1], B. Alper, H. Altmann, A. Andersen[14], P. Andrew, S.Ali-Arshad, W. Bailey, B. Balet, P. Barabaschi, Y. Baranov, P. Barker, R. Barnsley[2], M. Baronian, D.V. Bartlett, A.C. Bell, G. Benali, P. Bertoldi, E. Bertolini, V. Bhatnagar, A.J. Bickley, D. Bond, T. Bonicelli, S.J. Booth, G. Bosia, M. Botman, D. Boucher, P. Boucquey, M. Brandon, P. Breger, H. Brelen, W.J. Brewerton, H. Brinkschulte, T. Brown, M. Brusati, T. Budd, M. Bures, P. Burton, T. Businaro, P. Butcher, H. Buttgereit, C. Caldwell-Nichols, D.J. Campbell, D. Campling, P. Card, G. Celentano, C.D. Challis, A.V.Chankin[23], A. Cherubini, D. Chiron, J. Christiansen, P. Chuilon, R. Claesen, S. Clement, E. Clipsham, J.P. Coad, I.H. Coffey[24], A. Colton, M. Comiskey[4], S. Conroy, M. Cooke, S. Cooper, J.G. Cordey, W. Core, G. Corrigan, S. Corti, A.E. Costley, G. Cottrell, M. Cox[7], P. Crawley, O. Da Costa, N. Davies, S.J. Davies[7], H. de Blank, H. de Esch, L. de Kock, E. Deksnis, N. Deliyanakus, G.B. Denne-Hinnov, G. Deschamps, W.J. Dickson[19], K.J. Dietz, A. Dines, S.L. Dmitrenko, M. Dmitrieva[25], J. Dobbing, N. Dolgetta, S.E. Dorling, P.G. Doyle, D.F. Düchs, H. Duquenoy, A. Edwards, J. Ehrenberg, A. Ekedahl, T. Elevant[11], S.K. Erents[7], L.G. Eriksson, H. Fajemirokun[12], H. Falter, J. Freiling[15], C. Froger, P. Froissard, K. Fullard, M. Gadeberg, A. Galetsas, L. Galbiati, D. Gambier, M. Garribba, P. Gaze, R. Giannella, A. Gibson, R.D. Gill, A. Girard, A. Gondhalekar, D. Goodall[7], C. Gormezano, N.A. Gottardi, C. Gowers, B.J. Green, R. Haange, A. Haigh, C.J. Hancock, P.J. Harbour, N.C. Hawkes[7], N.P. Hawkes[1], P. Haynes[7], J.L. Hemmerich, T. Hender[7], J. Hoekzema, L. Horton, J. How, P.J. Howarth[5], M. Huart, T.P. Hughes[4], M. Huguet, F. Hurd, K. Ida[18], B. Ingram, M. Irving, J. Jacquinot, H. Jaeckel, J.F. Jaeger, G. Janeschitz, Z. Jankowicz[22], O.N. Jarvis, F. Jensen, E.M. Jones, L.P.D.F. Jones, T.T.C. Jones, J-F. Junger, F. Junique, A. Kaye, B.E. Keen, M. Keilhacker, W. Kerner, N.J. Kidd, R. Konig, A. Konstantellos, P. Kupschus, R. Lässer, J.R. Last, B. Laundy, L. Lauro-Taroni, K. Lawson[7], M. Lennholm, J.Lingertat[13], R.N. Litunovski, A. Loarte, R. Lobel, P. Lomas, M. Loughlin, C. Lowry, A.C. Maas[15], B. Macklin, C.F. Maggi[16], G. Magyar, V. Marchese, F. Marcus, J. Mart, D. Martin, E. Martin, R. Martin-Solis[8], P. Massmann, G. Matthews, H. McBryan, G. McCracken[7], P. Meriguet, P. Miele, S.F. Mills, P. Millward, E. Minardi[16], R. Mohanti[17], P.L. Mondino, A. Montvai[3], P. Morgan, H. Morsi, G. Murphy, F. Nave[27], S. Neudatchin[23], G. Newbert, M. Newman, P. Nielsen, P. Noll, W. Obert, D. O'Brien, J. O'Rourke, R. Ostrom, M. Ottaviani, S. Papastergiou, D. Pasini, B. Patel, A. Peacock, N. Peacock[7], R.J.M. Pearce, D. Pearson[12], J.F. Peng[26], R. Pepe de Silva, G. Perinic, C. Perry, M.A. Pick, J. Plancoulaine, J-P. Poffé, R. Pohlchen, F. Porcelli, L. Porte[19], R. Prentice, S. Puppin, S. Putvinskii[23], G. Radford[9], T. Raimondi, M.C. Ramos de Andrade, M. Rapisarda[29], P-H. Rebut, R. Reichle, S. Richards, E. Righi, F. Rimini, A. Rolfe, R.T. Ross, L. Rossi, R. Russ, H.C. Sack, G. Sadler, G. Saibene, J.L. Salanave, G. Sanazzaro, A. Santagiustina, R. Sartori, C. Sborchia, P. Schild, M. Schmid, G. Schmidt[6], H. Schroepf, B. Schunke, S.M. Scott, A. Sibley, R. Simonini, A.C.C. Sips, P. Smeulders, R. Smith, M. Stamp, P. Stangeby[20], D.F. Start, C.A. Steed, D. Stork, P.E. Stott, P. Stubberfield, D. Summers, H. Summers[19], L. Svensson, J.A. Tagle[21], A. Tanga, A. Taroni, C. Terella, A. Tesini, P.R. Thomas, E. Thompson, K. Thomsen, P. Trevalion, B. Tubbing, F. Tibone, H. van der Beken, G. Vlases, M. von Hellermann, T. Wade, C. Walker, D. Ward, M.L. Watkins, M.J. Watson, S. Weber[10], J. Wesson, T.J. Wijnands, J. Wilks, D. Wilson, T. Winkel, R. Wolf, D. Wong, C. Woodward, M. Wykes, I.D. Young, L. Zannelli, A. Zolfaghari[28], G. Zullo, W. Zwingmann.

PERMANENT ADDRESSES

1. UKAEA, Harwell, Didcot, Oxon, UK.
2. University of Leicester, Leicester, UK.
3. Central Research Institute for Physics, Budapest, Hungary.
4. University of Essex, Colchester, UK.
5. University of Birmingham, Birmingham, UK.
6. Princeton Plasma Physics Laboratory, New Jersey, USA.
7. UKAEA Culham Laboratory, Abingdon, Oxon, UK.
8. Universidad Complutense de Madrid, Spain.
9. Institute of Mathematics, University of Oxford, UK.
10. Freien Universität, Berlin, F.R.G.
11. Royal Institute of Technology, Stockholm, Sweden.
12. Imperial College, University of London, UK.
13. Max Planck Institut für Plasmaphysik, Garching, FRG.
14. Risø National Laboratory, Denmark.
15. FOM Instituut voor Plasmafysica, Nieuwegein, The Netherlands.
16. Dipartimento di Fisica, University of Milan, Milano, Italy.
17. North Carolina State University, Raleigh, NC, USA
18. National Institute for Fusion Science, Nagoya, Japan.
19. University of Strathclyde, 107 Rottenrow, Glasgow, UK.
20. Institute for Aerospace Studies, University of Toronto, Ontario, Canada.
21. CIEMAT, Madrid, Spain.
22. Institute for Nuclear Studies, Otwock-Swierk, Poland.
23. Kurchatov Institute of Atomic Energy, Moscow, USSR
24. Queens University, Belfast, UK.
25. Keldysh Institute of Applied Mathematics, Moscow, USSR.
26. Institute of Plasma Physics, Academica Sinica, Hefei, P. R. China.
27. LNETI, Savacem, Portugal.
28. Plasma Fusion Center, M.I.T., Boston, USA.
29. ENEA, Frascati, Italy.

At 1st July, 1992